

# Planar cell polarity signalling regulates cell adhesion properties in progenitors of the zebrafish laterality organ

Pablo Oteiza<sup>1,2,\*</sup>, Mathias Köppen<sup>3,4,\*</sup>, Michael Krieg<sup>5</sup>, Eduardo Pulgar<sup>1,2</sup>, Cecilia Farias<sup>1,2</sup>, Cristina Melo<sup>1,2</sup>, Stephan Preibisch<sup>3</sup>, Daniel Müller<sup>5</sup>, Masazumi Tada<sup>6</sup>, Steffen Hartel<sup>1,2</sup>, Carl-Philipp Heisenberg<sup>3</sup> and Miguel L. Concha<sup>1,2,†</sup>

## SUMMARY

Organ formation requires the precise assembly of progenitor cells into a functional multicellular structure. Mechanical forces probably participate in this process but how they influence organ morphogenesis is still unclear. Here, we show that Wnt11- and Prickle1a-mediated planar cell polarity (PCP) signalling coordinates the formation of the zebrafish ciliated laterality organ (Kupffer's vesicle) by regulating adhesion properties between organ progenitor cells (the dorsal forerunner cells, DFCs). Combined inhibition of Wnt11 and Prickle1a reduces DFC cell-cell adhesion and impairs their compaction and arrangement during vesicle lumen formation. This leads to the formation of a mis-shaped vesicle with small fragmented lumina and shortened cilia, resulting in severely impaired organ function and, as a consequence, randomised laterality of both molecular and visceral asymmetries. Our results reveal a novel role for PCP-dependent cell adhesion in coordinating the supracellular organisation of progenitor cells during vertebrate laterality organ formation.

**KEY WORDS:** Cell adhesion, PCP signalling, Organogenesis, Kupffer's vesicle, Left-right asymmetry, PCP signalling, Zebrafish

## INTRODUCTION

Epithelial organ morphogenesis is a key feature of metazoan development. Organ formation typically involves an initial stage of progenitor cell specification followed by a morphogenetic phase that gradually integrates progenitor cells into a functional supracellular structure (Wolpert, 2002). Tight coordination of adhesion, shape changes, polarisation and epithelialisation of progenitor cells is central to this process (Bryant and Mostov, 2008; Halbleib and Nelson, 2006) but how this is achieved *in vivo* remains unclear. Recent models of organogenesis in transparent embryos offer the opportunity to address this question by combining genetics, *in vivo* imaging and direct measurements of mechanical properties in progenitor cells (Krieg et al., 2008; Ulrich et al., 2005). One such model is the Kupffer's vesicle (KV), the first organ to be formed in the zebrafish embryo (D'Amico and Cooper, 1997; Essner et al., 2005).

KV is a ciliated epithelial organ homologous to the mouse ventral node and the *Xenopus* gastrocoel roof plate (Blum et al., 2007; Nonaka et al., 1998; Schweickert et al., 2007). In all of these embryonic structures, polarised cilia beating serves as a motor of directed extracellular fluid flow (the Nodal flow) that plays a crucial role in imposing the laterality of asymmetric gene expression and consequently organ chirality (Essner et al., 2005;

Kramer-Zucker et al., 2005). KV progenitor cells, the dorsal forerunner cells (DFCs), derive from dorsal marginal cells of the embryonic surface epithelium (enveloping layer, EVL), which ingress at the onset of epiboly and form a distinct cell cluster (D'Amico and Cooper, 1997; Oteiza et al., 2008). As epiboly progresses, the initially mesenchymal-like cluster becomes increasingly compact while remaining coupled to the EVL through a subset of polarised DFCs (Oteiza et al., 2008). At the end of epiboly, the cell cluster separates from the EVL, arranges into a rosette-like structure and generates a ciliated lumen at its apical centre (Oteiza et al., 2008). Hence, the formation of the KV involves a highly coordinated set of morphological events, such as cell polarisation, cell rearrangement, lumen formation and ciliogenesis (Oteiza et al., 2008). Despite recent advances in the molecular mechanisms of DFC specification (Amack et al., 2007; Amack and Yost, 2004; Oteiza et al., 2008), our understanding of the genetic and morphogenetic control of supracellular organisation during KV organogenesis remains very limited.

PCP signalling plays a key role in various developmental processes ranging from oriented cell division to collective cell migration (Wang and Nathans, 2007). Several lines of evidence indicate that the pathway affects these different processes by modulating cell polarisation and adhesion (Solnica-Krezel, 2006). Here, we show that a Wnt11- and Prickle1a-mediated PCP signalling pathway controls KV formation by facilitating the processes of lumen formation and ciliogenesis through modulation of adhesive properties between progenitor cells. We found that PCP-defective DFCs show reduced cell-cell adhesion, which results in impaired cluster compaction and organisation during vesicle formation. This leads to compromised lumen expansion and ciliogenesis and the failure to generate a Nodal flow that is sufficient to impose laterality on embryo asymmetry. Our results show that adhesion between organ progenitor cells serves to coordinate embryonic organogenesis and provide novel insights into the role of PCP signalling in laterality organ formation.

<sup>1</sup>Anatomy and Developmental Biology Program, Institute of Biomedical Sciences, University of Chile, Santiago 8380453, Chile. <sup>2</sup>Millennium Nucleus of Neural Morphogenesis (NEMO), Santiago 8380453, Chile. <sup>3</sup>Max Planck Institute of Molecular Cell Biology and Genetics, 01307 Dresden, Germany. <sup>4</sup>Instituto Gulbenkian de Ciéncia, Lisbon, P-2781-901 Oeiras, Portugal. <sup>5</sup>Biotec, Technische Universität Dresden, 01062 Dresden, Germany. <sup>6</sup>Department of Cell and Developmental Biology, University College London, London WC1E 6BT, UK.

\*These authors contributed equally to this work

†Author for correspondence ([mconcha@med.uchile.cl](mailto:mconcha@med.uchile.cl))

## MATERIALS AND METHODS

### Zebrafish lines

The following zebrafish (*Danio rerio*) lines and alleles were used: wild-type TL, *Tg(sox17::GFP)* (Sakaguchi et al., 2006); *Tg(β-actin::HRAS-EGFP)* (Cooper et al., 2005); *slbx<sup>a226</sup>* (Heisenberg et al., 1996); *ppt<sup>a98</sup>* (Hammerschmidt et al., 1996); and *slbx<sup>a226</sup>, ppt<sup>a98</sup>* (Kilian et al., 2003). Embryos were grown at 31°C unless otherwise indicated, manipulated in E3 zebrafish embryo medium or Danieau buffer and staged according to morphology (Kimmel et al., 1995) and age (hours past fertilisation, hpf).

### Morpholino injections

The following morpholino oligonucleotides (MO) were used: *pk1aMOATG1* and *pk1aMOATG1*fluo (5'-GCCACCGTGATTCTC-CAGCTCCAT-3') (Carreira-Barbosa et al., 2003); *pk1aMOATG1-4b* (5'-GCCGCCCCATGATTCTCAACTTCAT-3'); *pk1aMOATG2* (5'-CAGCTCCATCACTAAACACCCCCCTCA-3') (Veeman et al., 2003); *pk1aMOATG2-5b* (5'-CACCTCGATCAGTAACACGCCGTCA-3'); and *e-cad-MO* (5'-ATCCCACAGTTGTTACACAAGCCAT-3') (Babb and Marrs, 2004). Embryos were injected at the 1-cell stage as previously described (Barth and Wilson, 1995). Yolk syncytial layer (YSL) injection of fluorescently labelled MOs was performed at approximately the 1000-cell stage (Amack and Yost, 2004). The presence of the MO in DFCs was verified during gastrulation stages using a fluorescence-dissecting microscope. Heart loop laterality was scored between 36 and 40 hpf on a dissecting scope.

### In situ hybridisation

Wholemount *in situ* hybridisation was performed as previously described (Barth and Wilson, 1995). Antisense RNA probes were synthesised from partial cDNAs of *pk1a* (Carreira-Barbosa et al., 2003), *wnt11* (Heisenberg et al., 2000), *wnt5* (Kilian et al., 2003), *cmlc2* (*myl7* – Zebrafish Information Network) (Echeverri and Oates, 2007), *lefty2* and *southpaw* (Long et al., 2003). After staining, embryos were embedded in 70% glycerol and photographed on an Olympus S2X12 dissecting scope using Spot Advanced software. For sectioning, embryos were embedded in a 10:1 gelatin:albumen solution. Polymerisation was induced by adding one volume of glutaraldehyde and embryos were oriented in pockets for sectioning. Sections of 10–20 µm were made using a Leica VT1000S Vibratome and photographed on a Zeiss Axioplan-2 microscope using MetaView software. Images were imported into Adobe Photoshop. For these and all other experiments, image manipulation was limited to adjustment of levels, colour balance, contrast and brightness.

### Immunohistochemistry

Embryos between gastrulation and the 2-somite stage were stained as described previously (Oteiza et al., 2008). These embryos were mounted on agarose-coated dishes in PBS-Triton medium or embedded in 1% low-melting-point agarose. Embryos at the 6- to 8-somite stage were fixed overnight at 4°C in 4:1 methanol:DMSO and then stained as described (Koppen et al., 2006). To image Kupffer's vesicle, the tip of the tail was dissected and embedded in 1% agarose. The following primary antibodies and dilutions were used: mouse anti-ZO-1 (Invitrogen, 1:200); mouse anti-acetylated α-tubulin (Sigma, 1:400); and rabbit anti-zebrafish E-cadherin [(Babb and Marrs, 2004) 1:200]. Samples were imaged on a Zeiss LSM META confocal microscope using an Achroplan 40×/0.8 W dipping objective or a Plan-APOCHROMAT 40×/1.2 W objective.

### Image quantification

Morphologic and volumetric analysis of KV lumen was performed by generating 3D reconstructions of anti-ZO-1 stainings using Volocity software (Improvision). KV cilia length measurements were performed on *z*-projections of dorsal confocal stacks of embryos stained with anti-acetylated α-tubulin. The number of DFCs during epiboly was determined using Imaris software (Bitplane AG). Fluorescent beads were pressure-injected into the KV as previously described (Essner et al., 2005). Four control and five *pk1a-MO* embryos were analysed. Tracking of fluorescent beads was performed using IDL software. To determine average anti-ZO-1 distribution within the DFC cluster, confocal stacks of multiple 1-somite stage *Tg(sox17::GFP)* embryos (control, 12 embryos; *pk1a-MO*, 16 embryos) were manually

registered by their centre of gravity. All images were then fused into a single 3D image by averaging. Images were filtered with a small Gaussian kernel prior to 3D reconstruction using Volocity software (Improvision) to suppress noise and artefacts owing to different image backgrounds.

### Live imaging

Embryos from *Tg(sox17::GFP)* in-crosses or crosses between *Tg(sox17::GFP)* and *Tg(β-actin::HRAS-EGFP)* fish were manually dechorionated and mounted in 0.5% low-melting-point agarose just prior to imaging. Time-lapse, multiple-focal-plane (4D) microscopy was then performed at 22°C on a BioRad Radiance 2000 multi-photon system using a Plan Apochromat 60×/1.2 W objective. Movies were processed using Volocity software (Improvision).

### Single-cell adhesion measurements

To perform single-cell adhesion measurements, DFCs were isolated from dissociated *Tg(sox17::GFP)* embryos at 75% epiboly. Dissociation was performed by first dechorionating approximately 100 embryos enzymatically using 10 mg/ml pronase in sterilised E2 buffer. After several washing steps in sterilised E2 buffer, embryos were gently mixed in DMEM/F-12 + 0.5 mg/ml EDTA solution to obtain single cells. Cells were then harvested by centrifugation at 600 rpm (40 g) for 1 minute and were then transferred to fresh DMEM/F-12 + Pen-Strep solution in a 5 ml Falcon tube. Fluorescent DFCs were automatically isolated using a FACSaria cell sorting system (BD Biosciences). Cells were then used for single-cell force spectroscopy (CellHesion, JPK Instruments, Berlin, Germany). Using plasma-activated cantilevers (Veeco NP-0, nominal spring constant  $k=60$  mN/m), cells were incubated in 2.5 mg/ml concanavalin A (ConA, Sigma) overnight at 4°C and rinsed in 1× PBS prior to use. Plasma-activated microscope slides (GoldSeal) were prepared using a two-well coating mask (nAmbition) to obtain an adhesive and non-adhesive substrate. One well was filled with 50 µl of heat-inactivated foetal calf serum (Invitrogen) to passivate the surface (nonadhesive substrate). The other well was filled with 50 µl of 2.5 mg/ml ConA (adhesive substrate). Prior to the experiment, the substrate was rinsed with the cell culture medium used to perform the adhesion tests (CO<sub>2</sub>-independent DMEM/F-12, buffered 1:1 with 15 mM Hepes and supplemented with Pen-Strep solution). Diluted cell suspensions were then seeded onto the substrate. All experiments were carried out at 25°C. Cells expressing strong levels of GFP were selected using epifluorescence microscopy. A ‘probe’ cell was picked from the non-adhesive side of the substrate using a ConA-decorated cantilever by gently pressing on the cell with a controlled force of 1 nN. The cell was then positioned away from the surface for 2–10 minutes to ensure firm attachment to the cantilever. The probe cell was then aligned above a ‘target’ cell that was firmly attached to the adhesive ConA-decorated area of the substrate. Adhesion measurements (‘force-distance cycles’) were performed using 1 nN contact force, 10 µm/second approach and retraction velocity, and contact times of 5 and 10 seconds. The order of these two contact time conditions was varied randomly for each pair of cells to prevent systematic bias or history effects. Each condition was repeated up to three times for each cell pair, with a resting time of more than 10 seconds between successive contacts. Each probe cell was used to test several target cells. Calcium-dependence of cell adhesion was tested after depleting calcium by adding 5 mM EGTA (Sigma) to the medium. Force-distance curves were analysed using IgorPro custom-made routines to extract the maximum adhesion force. The data was then pooled and statistically processed. The median ± m.a.d. [median absolute deviation: median (xi-x̄)] were extracted with a custom IgorPro (WaveMetrics) function and used in KaleidaGraph (SynergySoftware) for Wilcoxon statistical significance tests with a *P*-value cut-off of 0.01. Force and number of small unbinding events were extracted using a home-written procedure in IgorPro. Histograms were compiled with a bin-size e<sup>0.25x</sup> or e<sup>0.5x</sup> with x=1,2,3...n. Frequency distributions [P(F)] were fitted to a log-normal probability density function

$$P(F) = A \exp \left[ - \left( \frac{\ln \left( \frac{F}{F_{avg}} \right)}{\omega} \right)^2 \right] \quad (1)$$

to extract mean unbinding force ( $F_{avg}$ ), where  $F$  is the force,  $A$  is the amplitude and  $\omega$  is the width of the distribution. The width of the distribution is related to the standard deviation as follows:

$$\sigma = \sqrt{\exp[2 \times \ln(F_{avg}) + \omega^2] \times [\exp(\omega^2) - 1]} . \quad (2)$$

## RESULTS

### Wnt11 and Prickle1a are expressed in the dorsal forerunner cells and regulate Kupffer's vesicle morphogenesis

To investigate a possible role for PCP signalling during KV organ morphogenesis, we first determined the expression of PCP components in DFCs by wholemount *in situ* hybridisation. We found that the secreted ligand *wnt11* (Heisenberg et al., 2000) and the core signalling component *prickle1a* (*pk1a*) (Carreira-Barbosa et al., 2003; Veeman et al., 2003), but not the related ligand *wnt5* (Kilian et al., 2003), are expressed in KV progenitor cells (Fig. 1A-C). These observations strongly suggest a possible role for Wnt11 and Pk1a, but not of Wnt5, in KV morphogenesis.

To test whether Wnt11 and Pk1a participate in KV formation, we examined vesicle lumen shape at the 8-somite stage, when Nodal flow occurs (Essner et al., 2005; Kramer-Zucker et al., 2005). In wild-type embryos, the KV appeared as a flattened sphere with a single lumen (Fig. 1D,G). Although no clear morphological defects were observed in the KV of *wnt11* [*silverblick* (*slb*)] (Heisenberg et al., 2000) and *wnt5* [*pipetail* (*ppt*)] (Kilian et al., 2003) mutant embryos, embryos injected with morpholinos (MO) targeting the ATG initiation codon of *pk1a* (*pk1a-MOATG1*) (Carreira-Barbosa et al., 2003) presented a markedly smaller, frequently mis-shapen and fragmented lumen (Fig. 1E-I). Similar results were obtained using a second *pk1a*-targeting MO (*pk1a-MOATG2*) (Veeman et al., 2003), whereas a corresponding mispair MO (mispair-MO) did not cause major morphological defects (data not shown). This finding strongly suggests that *pk1a* morphant phenotypes result from specific inactivation of the *pk1a* gene. All subsequent analyses were performed using *pk1a-MOATG1*, and morphant embryos are referred to as *pk1a-MO* embryos in the following text.

Interestingly, a low dose of *pk1a-MO* that was ineffective in wild-type embryos induced clear alterations in KV shape when injected into *slb* mutants (Fig. 1J). The specificity of this genetic interaction was confirmed by the absence of major defects in the KV of *ppt* mutant embryos injected with low doses of *pk1a-MO* and in the *slb;ppt* double mutant (Fig. 1J). This suggests that Wnt11 and Pk1a, but not Wnt5, have partially redundant functions in KV organogenesis. To determine if PCP function is specifically required in DFCs for proper KV morphogenesis, we knocked down Pk1a in DFCs alone by injecting *pk1a-MO* into the yolk syncytial layer (YSL) of mid-blastula stage embryos (Amack and Yost, 2004). This treatment induced the appearance of clear morphological abnormalities in the KV lumen of both wild-type and *slb* embryos (Fig. 1J), indicating that Wnt11- and Pk1a-mediated PCP signalling is required specifically in DFCs during KV organogenesis. In summary, these findings indicate that Wnt11- and Pk1a-mediated PCP signalling in DFCs regulates KV lumen morphogenesis in zebrafish.

### PCP signalling regulates KV lumen volume, ciliation and function

To gain better insights into the organogenetic role of PCP signalling, we carefully quantified the effects of *pk1a* inhibition on lumen volume and ciliation. Whereas control vesicles developed an oval

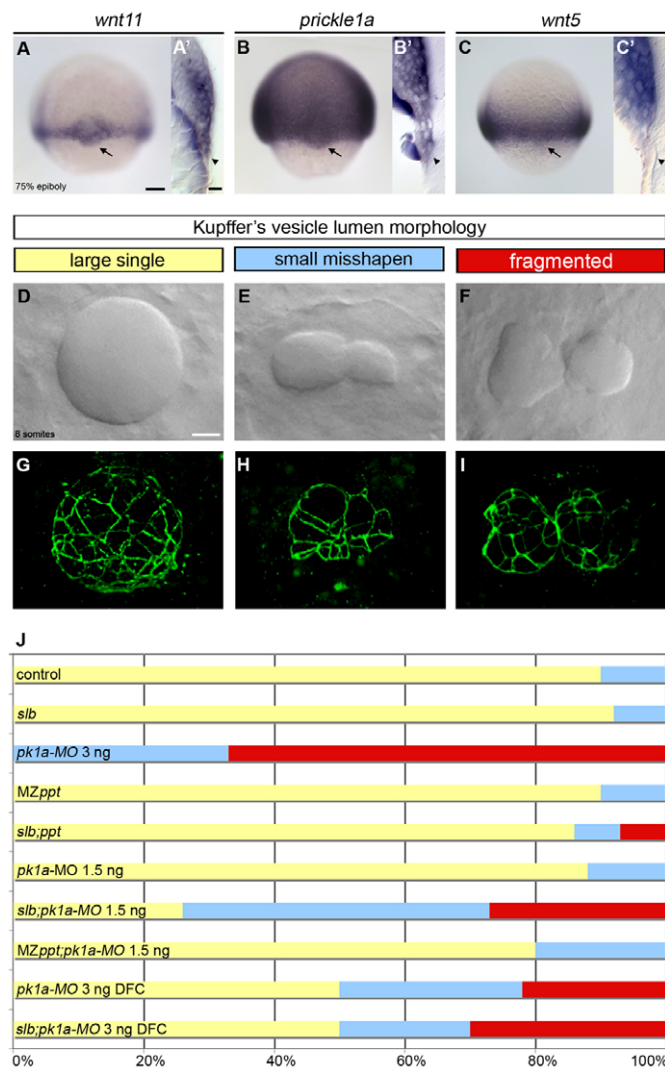


**Fig. 1. The PCP signalling components *wnt11* and *prickle1a* are expressed in the DFCs and control KV morphogenesis.**

(A-C') Expression of *wnt11*, *pk1a* and *wnt5* in wild-type zebrafish embryos at 75% epiboly as revealed by wholemount *in situ* hybridisation. Arrows in dorsal views (A,B,C) and arrowheads in sagittal sections (A',B',C') point to the dorsal forerunner cell (DFC) expression domain. (D-I) Kupffer's vesicle (KV) lumen morphologies at the 8- to 10-somite stage in wild-type (D,G) and *wnt11*- and *pk1a*-defective (E,F,H,I) embryos. (D-F) DIC microscopy views of KV in living embryos. (G-I) Three-dimensional projections of confocal stacks through the entire KV stained with anti-ZO-1 antibody, outlining lumen shape. (J) Horizontal bar chart of the relative frequency of the three main KV morphological phenotypes (large single lumen, yellow; small misshapen lumen, blue; fragmented lumen, red) scored in different experimental conditions: control (wild-type untreated,  $n=21$ ); *slb* [*wnt11* (*silverblick*) mutants,  $n=12$ ]; *pk1a-MO* 3 ng (wild-type injected with 3 ng of *pk1a-MO* at the 1-cell stage,  $n=9$ ); *MZppt* [maternal zygotic *wnt5* (*pipetail*) mutants,  $n=10$ ]; *slb;ppt* (*wnt11;slb* and *wnt5;ppt* double mutants,  $n=14$ ); *pk1a-MO* 1.5 ng (wild-type injected with 1.5 ng of *pk1a-MO* at the 1-cell stage,  $n=8$ ); *slb;pk1a-MO* 1.5 ng (*slb* mutants injected with 1.5 ng of *pk1a-MO* at the 1-cell stage,  $n=19$ ); *MZppt;pk1a-MO* 1.5 ng (*MZppt* injected with 1.5 ng of *pk1a-MO* at the 1-cell stage,  $n=10$ ); *pk1a-MO* 3 ng DFC [abrogation of *pk1a* in wild-type DFCs by injection of 3 ng of *pk1a-MO* in the yolk syncytial layer (YSL) at mid-blastula stages,  $n=18$ ]; and *slb;pk1a-MO* 3 ng DFC (abrogation of *pk1a* in *slb* DFCs by injection of 3 ng of *pk1a-MO* in the YSL at midblastula stages,  $n=10$ ). Scale bars: 20  $\mu$ m.

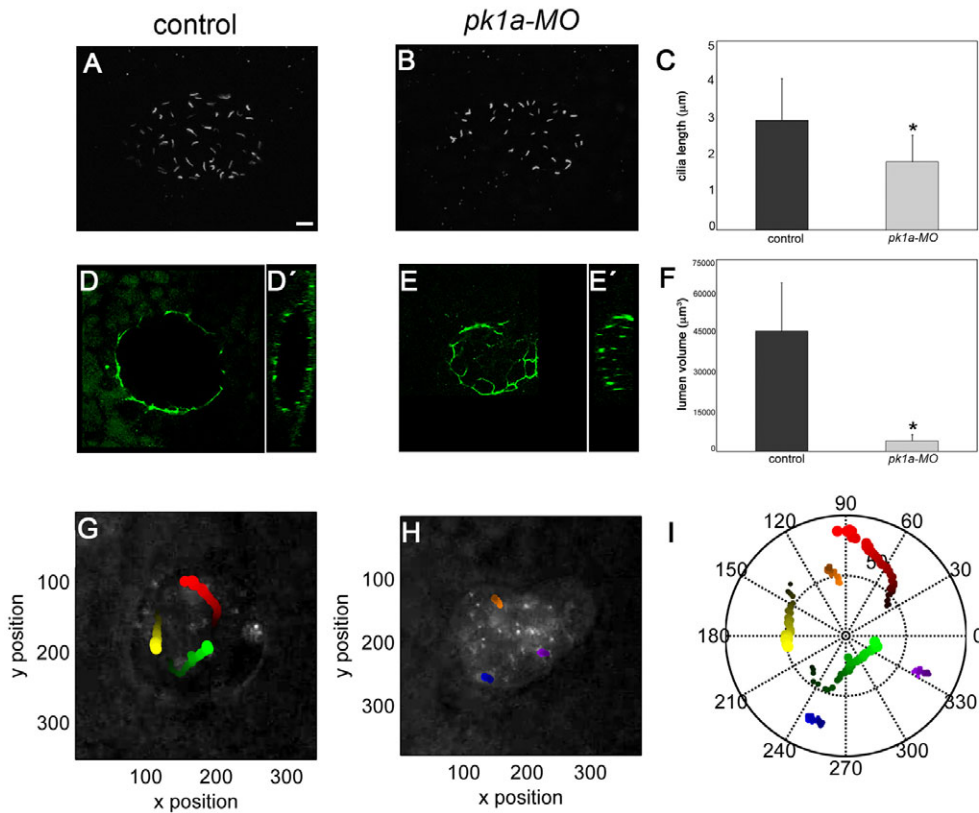


**Fig. 2. PCP signalling regulates cilia length, lumen volume and Nodal flow in the KV.** (A-C) Comparison of cilia length of control and *pk1a*-MO-injected 8-somite stage zebrafish embryos. z-projections of a dorsal confocal stack through the KV of a control (A) and a morphant (B) embryo stained with an anti-acetylated  $\alpha$ -tubulin antibody reveal a more unevenly shaped lumen and shorter cilia in the morphant. Quantitative analysis of multiple embryos (C) reveals significantly shorter cilia in *pk1a*-MO embryos compared with controls (mean  $\pm$  s.d.; n=5 control embryos and 3 morphants; \*, P<0.05, Student's t-test). (D-E') Anti-ZO-1 staining of the KV in control and *pk1a*-MO-injected embryos. Single dorsal focal planes at the centre of the vesicle (D,E) and sagittal views (D',E') are shown. (F) KV lumen volume is reduced in *pk1a*-MO embryos compared with controls [mean  $\pm$  s.d.; n=10 control embryos and 5 morphants; \*, P<0.05, Student's t-test (KaleidaGraph, SynergySoftware)]. Approximate volume was determined based on the three main axes of the ellipsoid lumen. For fragmented lumina, volume was computed as the sum. (G-I) Nodal flow is strongly reduced in *pk1a*-MO embryos. Colour-coded tracks of fluorescent beads injected into the KV of a control (G) and a *pk1a*-MO (H) embryo. The bead trajectories shown in G and H are plotted in I. Scale bars: 20  $\mu$ m.

lumen that rapidly expanded during somitogenesis, the lumen of *pk1a*-MO embryos was markedly flatter and reduced in volume (Fig. 2D-F). Similarly, the number and final length of cilia was also significantly reduced (Fig. 2A-C; see Fig. S1 in the supplementary material), suggesting a functional link between lumen formation and ciliation.

To address whether the observed defects of *pk1a*-MO embryos correlate with impaired KV function, we analysed Nodal flow within the vesicle by injecting fluorescent beads directly into the lumen. As previously described (Essner et al., 2005; Kramer-Zucker et al., 2005), beads injected into control vesicles underwent counterclockwise movement (Fig. 2G,I; see Movie 1 in the supplementary material). On the contrary, beads in *pk1a*-MO embryos showed only Brownian motion with no clear directionality (Fig. 2H,I; see Movie 2 in the supplementary material). In summary, these results indicate that PCP signalling controls KV organ function by regulating KV lumen formation and ciliation.

### PCP signalling regulates the laterality of visceral asymmetries

Nodal flow has been widely described as a key player during the establishment of embryonic left-right asymmetries (Nonaka et al., 2002; Nonaka et al., 1998; Schweickert et al., 2007). To analyse the

consequences of defective KV organogenesis in zebrafish body handedness, we examined the orientation of heart looping, the first anatomical asymmetry of the vertebrate embryo (Brown and Wolpert, 1990). In wild-type embryos, heart looping is usually oriented to the right (Fig. 3A). Interestingly, and in concordance with our analysis of KV shape, we observed that combined inhibition of Wnt11 and Pk1a, but not Wnt5, led to randomisation of heart loop laterality (Fig. 3B-D). Moreover, similar defects were also observed when abrogation of Pk1a function was restricted to DFCs (Fig. 3D).

To better understand the underlying mechanism of this phenotype, we analysed the asymmetric expression of Nodal signalling in the lateral plate mesoderm (LPM), a well-described molecular response to Nodal flow that precedes anatomical asymmetries in vertebrates (Hamada et al., 2002). In wild-type embryos, the Nodal ligand *southpaw* and the diffusible negative regulator of the pathway *lef1y2* are both expressed on the left LPM (Long et al., 2003) (see Fig. S2 in the supplementary material). We observed that abrogation of Wnt11- and Pk1a-mediated PCP signalling led to randomisation of the asymmetric expression of both *southpaw* and *lef1y2* (see Fig. S2 in the supplementary material). In summary, these results indicate that PCP signalling participates in the establishment of zebrafish visceral asymmetries by regulating asymmetric Nodal expression.

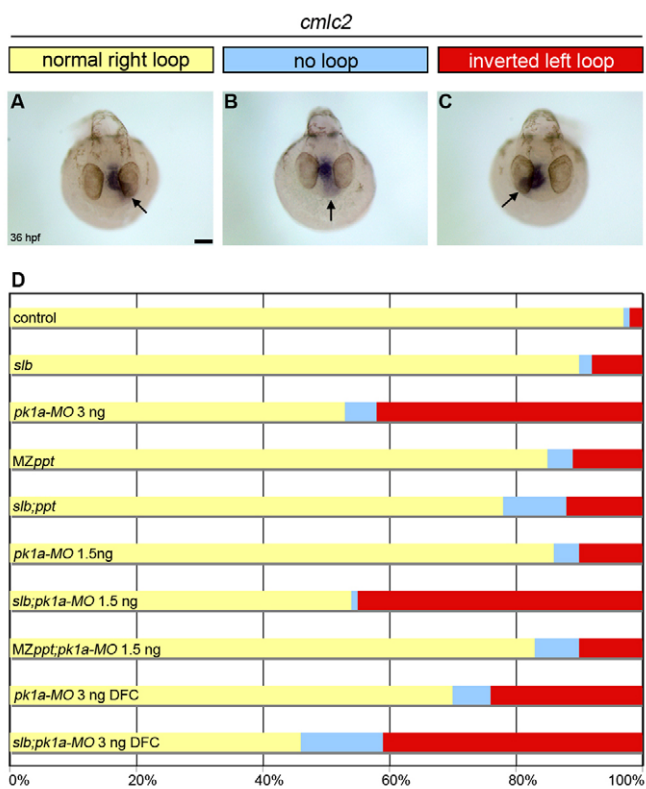


**Fig. 3. PCP signalling regulates heart loop laterality in zebrafish.** (A–C) Top view of 36 hpf *pk1a-MO*-injected embryos showing expression of *cardiac myosin light chain 2* (*cmlc2*) in the heart tube by wholemount *in situ* hybridisation. Arrows indicate the orientation of heart looping: normal loop to the right (A), absent loop (B) and inverted loop to the left (C). (D) Horizontal bar chart of the relative frequency of heart loop orientation (right loop, yellow; no loop, blue; left loop, red) scored in different experimental conditions (same conditions as in Fig. 1: control ( $n=122$ ); *slb* ( $n=12$ ); *pk1a-MO* 3 ng ( $n=137$ ); *MZppt* ( $n=122$ ); *slb;ppt* ( $n=50$ ); *pk1a-MO* 1.5 ng ( $n=94$ ); *slb;pk1a-MO* 1.5 ng ( $n=170$ ); *MZppt;pk1a-MO* 1.5 ng ( $n=60$ ); *pk1a-MO* 3 ng DFC ( $n=46$ ); and *slb;pk1a-MO* 4 ng DFC ( $n=56$ ). Scale bar: 20  $\mu$ m.

### PCP signalling coordinates DFC compaction and KV lumen expansion

KV morphogenesis involves the transformation of an initially flat array of mesenchymal-like DFCs into an epithelial vesicle (Oteiza et al., 2008). To understand how PCP abrogation leads to defects in this process, we performed multi-photon time-lapse imaging and immunostaining of control and *pk1a-MO*-injected *Tg(sox17::GFP)* embryos. As we have previously described, in control embryos, DFCs arrange into a broad group of 20–30 mesenchymal-like cells adjacent to the dorsal germ ring at the onset of gastrulation (Oteiza et al., 2008). During epiboly, the DFC cluster undergoes progressive compaction while being coupled to the EVL through distinct groups of polarised bottle-shaped DFCs (Oteiza et al., 2008) (Fig. 4A,A',G). After reaching the vegetal pole at the end of epiboly, the cluster becomes separated from the overlying dorsal marginal EVL. During this separation, the apices of bottle-shaped DFCs turn towards the inside of the cluster and generate multiple 3D rosette structures around ZO-1-rich apical focal points. These rosette structures then rearrange into a single rosette followed by the formation of a rapidly expanding lumen at the apical centre (Fig. 4C,C',E,E',G) (Oteiza et al., 2008).

In *pk1a-MO* embryos, we observed that the initial arrangement, number and morphological appearance of mesenchymal DFCs was comparable to that of untreated embryos (data not shown). Likewise, the attachment of bottle-shaped DFCs to the EVL via tight junctions occurred as in controls (Fig. 4B,B'), indicating that DFC specification and polarisation does not depend on Pk1a activity. However, convergence and integration of the cells into a compact cluster frequently failed (see Movie 3 in the supplementary material). At 80% epiboly, DFC cluster width was significantly greater in *pk1a-MO* embryos compared with controls, whereas total cell number was not increased (Fig. 4B,B',H,I). After subsequent cluster separation from the EVL, cells arranged into multiple, widely spaced epithelial rosettes that frequently failed to coalesce into a single rosette between 100% epiboly and 1-somite stages (Fig. 4D,D'; see Fig. S3 and Movie 4 in the supplementary material). Importantly, during the stages of lumen opening, we observed that widely spaced rosettes of *pk1a-MO* embryos presented a clear reduction in the number of DFCs facing the KV lumen compared with controls (Fig. 5A–I). This decrease in the number of lumen-forming DFCs in *pk1a-MO* embryos was accompanied by a decreased rate of lumen expansion during KV formation (Fig. 5E–H,J,K), a feature that is consistent with the defects in KV lumen shape detected at the 2-somite (Fig. 4F,F') and 8-somite (Fig. 1E,F,H,I; Fig. 2D–F) stages. To determine whether the observed decrease in lumen expansion was a consequence of defective apical growth in DFCs, we measured the contribution of the apical domain of lumen-facing DFC to KV lumen expansion (Fig. 5L). Interestingly, we observed that although the rate of lumen growth was strongly reduced in *pk1a-MO* embryos (Fig. 5K), the average apical growth of lumen-facing DFCs did not differ accordingly between *pk1a-MO* and control embryos (Fig. 5L). This observation strongly suggests that the main cause of defective lumen expansion in *pk1a-MO* embryos is the reduced number of lumen-forming DFCs. In summary, these results show that PCP signalling coordinates KV organ morphogenesis by regulating convergence and organisation of DFCs during vesicle lumen expansion.

### PCP signalling regulates cell-cell adhesion properties between DFCs

PCP signalling participates in many different morphogenetic processes from flies to mammals (Seifert and Mlodzik, 2007). Although the cellular response to PCP signalling in these systems seems to be highly variable, an emerging possibility is that PCP signalling acts in different contexts by regulating cell-cell adhesion (Zallen, 2007). To determine whether the loosening of the DFC cluster induced by PCP abrogation was due to reduced adhesion properties between DFCs, we directly measured their adhesion properties using single-cell force spectroscopy (SCFS) (Puech et al., 2006) (Fig. 6A). We specifically isolated DFCs from control and *pk1a-MO* gastrula stage *Tg(sox17::GFP)* embryos via fluorescence-activated cell sorting (FACS), placed them in culture and recorded maximum adhesion force and quantified unbinding events (Fig. 6B; see Materials and methods for details). Importantly, we found that the adhesion force between DFCs isolated from *pk1a-MO* embryos was significantly reduced when compared with control DFCs for both 5 and 10 seconds of contact time ( $P<0.001$ ; Fig. 6C,D).

To gain further insights into the mechanisms by which PCP signalling modulates DFC adhesion properties, we next analysed the strength of single unbinding events displayed as ‘steps’ in each force curve (Fig. 6B). Based on the mechanical coupling of cell

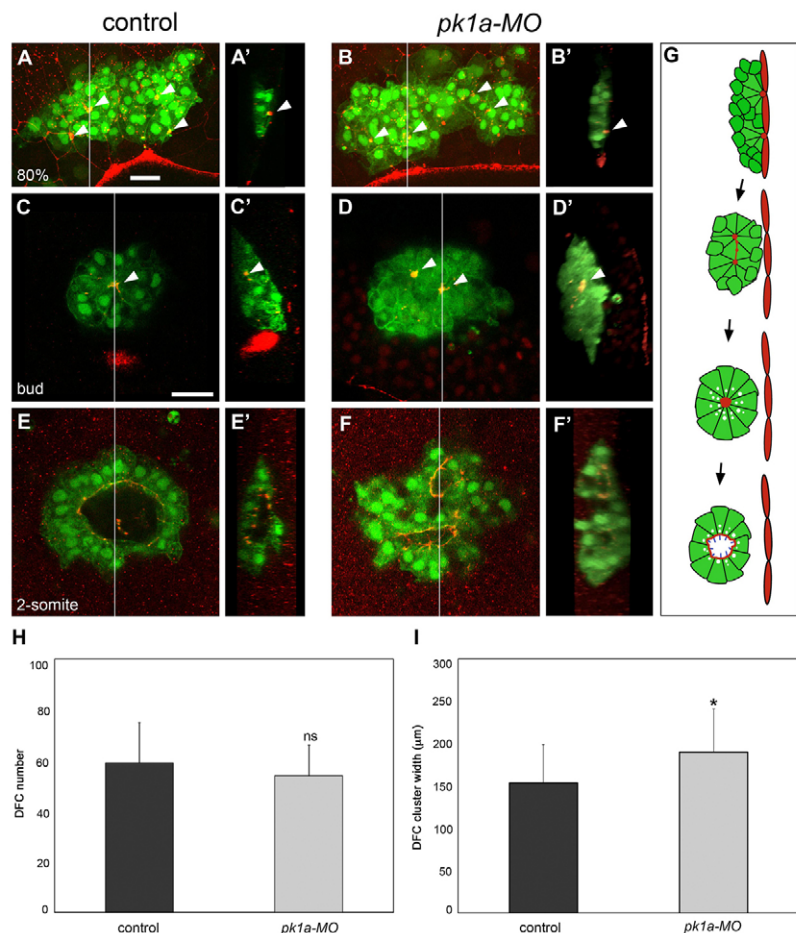


**Fig. 4. Pk1a is required for DFC cluster organisation and KV lumen morphogenesis.** (A–B') DFC cluster organisation at 80% epiboly in control and *pk1a*-MO-injected zebrafish embryos expressing *sox17::GFP* and immunostained with anti-ZO-1 antibody. Dorsal projections of confocal z-stacks (A,B) and sagittal views at the position of the line (A',B'; embryo surface to the right) are shown. Animal pole is to the top. In a control embryo, DFCs form a compact cluster that is in contact with the interior surface of the enveloping layer (EVL) close to the margin. Anti-ZO-1 staining reveals distinct accumulations of ZO-1 that mark contact points (arrowheads) between DFCs and the overlying EVL (A,A'). In a *pk1a*-MO embryo, the DFC cluster is wider and more irregularly shaped than in the control. ZO-1-rich attachment points (arrowheads), similar to those of the control, are observed (B,B'). (C–F') DFC cluster organisation at bud and 2-somite stages in control and *pk1a*-MO embryos expressing *sox17::GFP* and immunostained with anti-ZO-1 antibody. Single focal planes at the centre of the cluster (C–F) and sagittal views of the cluster at the position of the line (C'–F'; embryo surface to the right) are shown. Anterior is to the top. In a bud-stage control embryo, a single major focal point enriched for ZO-1 (arrowheads) is seen at the centre of the cluster (C,C'). The cluster is disconnected from the overlying EVL (C'). In a bud-stage *pk1a*-MO embryo, two major focal points are observed within the cluster (D,D'; arrowheads). In a 2-somite stage control embryo, a single large lumen is seen in the interior of the DFC cluster and is delineated by anti-ZO-1 signal (E,E'). A 2-somite stage *pk1a*-MO embryo shows two distinct lumina (F,F'). (G) Schematic representation of KV lumen formation. (H) Graphic representation of DFC number (mean  $\pm$  s.d.;  $n=24$  control and  $n=22$  *pk1a*-MO embryos;  $P<0.01$ ). (I) Graphic representation of DFC cluster width (mean  $\pm$  s.d.;  $n=29$  control and 29 *pk1a*-MO embryos; \*,  $P<0.01$ ). ns, not significant. Scale bars: 30  $\mu$ m.

adhesion molecules to the cell body, it is possible to distinguish between two different bond properties, ‘tethers’ and ‘jumps’. At cell separations larger than 10  $\mu$ m, cell adhesion molecules adhering to each other are detached from the intracellular actin cytoskeleton (Evans et al., 2005; Muller et al., 2009). In such situations, pulling on cell adhesion molecules results in extruding a lipid-nanotube or membrane tether from the plasma membrane (Fig. 6B, inset). This force is mainly determined by membrane mechanical properties such as membrane tension and membrane-cytoskeleton anchoring (Sheetz, 2001; Sun et al., 2007). We observed that tether number was comparable with that of controls, whereas tether forces were reduced in *pk1a*-MO DFCs (Fig. 6F), indicating that PCP signalling might regulate membrane

properties in DFCs (see Discussion). The second bond property amenable to be analysed by SCFS occurs at close distance to the contact point (up to 6–10  $\mu$ m). In this case, unbinding events are characterised by a spring-like extension (‘jump’) with a linearly increasing force before bonds break (Panorchan et al., 2006; Taubenberger et al., 2007) (Fig. 6B, inset). In such a case, bonds remain coupled to the intracellular cytoskeleton (Muller et al., 2009) and their forces are determined by the binding strength of cell adhesion molecules to its ligand (Evans, 2001), the clustering of adhesion molecules (Taubenberger et al., 2007; Tulla et al., 2008) and the intracellular coupling of adhesion molecules to the cytoskeleton (Puech et al., 2006). Although we observed a slight increase in the number of jumps in *pk1a*-MO versus control cells

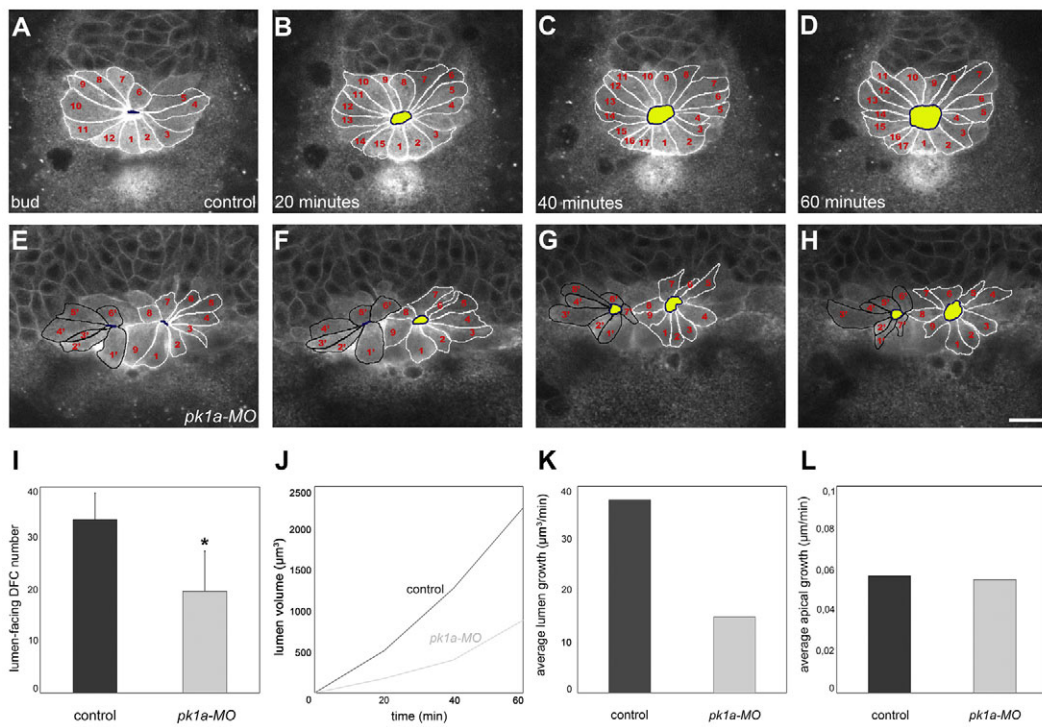


**Fig. 5. Pk1a regulates KV lumen formation and expansion.** (A–H) Live imaging of KV lumen formation in control and *pk1a*-MO zebrafish embryos coexpressing *sox17::GFP* and  $\beta$ -actin::HRAS-EGFP. Single focal planes at the centre of the DFC cluster are shown, beginning at the tailbud stage and followed every 20 minutes as indicated. Anterior is to the top. Each lumen-forming DFC is outlined and numbered. DFC apical sides are outlined in blue and the lumen is highlighted in yellow. (I) Graphic representation of lumen-forming DFC number in control and *pk1a*-MO embryos (mean  $\pm$  s.d.;  $n=6$  control and 7 *pk1a*-MO embryos; \*,  $P<0.01$ , Student's *t*-test) obtained from nuclei-stained *Tg(sox17::GFP)* embryos. (J) Graphic representation of lumen expansion during early KV formation as measured in *Tg(sox17::GFP;β*-actin::HRAS-EGFP) embryos. Approximate volume for control ( $n=2$  movies) and *pk1a*-MO ( $n=2$  movies) embryos was determined based on the three main axes of the ellipsoid lumen at different time-points. The start point was set at lumen opening. For fragmented lumina, volume was computed as the sum. (K) Graphic representation of the average rate of lumen growth (final volume/total time) based on the data presented in J. (L) Graphic representation of lumen-facing DFC average rate of apical growth [final lumen circumference/final number of lumen-forming DFCs/total time] measured in *Tg(sox17::GFP;β*-actin::HRAS-EGFP) embryos. Scale bar: 20  $\mu$ m.

(Fig. 6F, inset), the distribution of the jump forces analysed in each force curve was extremely right-tailed to larger forces and their logarithm was normally distributed (Fig. 6E). Importantly, fitting the data to a log-normal distribution (see Materials and methods), we estimated that the mean force required to break cytoskeleton-coupled jumps was reduced two-fold from 200 pN in wild-type to 100 pN in *pk1a*-MO DFCs (Fig. 6F; see Materials and methods). These results strongly suggest that the reduction in adhesion forces between *pk1a*-MO DFCs (Fig. 6D) might be caused by defects in cooperativity and strengthening of adhesion bonds (Fig. 6F; see Discussion).

Importantly, our SCFS measurements showed that adhesion force between DFCs is reduced to background levels in the presence of the calcium chelator EGTA (Fig. 6D). Thus, we next explored the role of E-cadherin, a calcium-dependent adhesion molecule strongly expressed in the DFCs (Kane et al., 2005) (data not shown), in KV organogenesis. As expected, we observed that abrogation of E-cadherin using a previously characterised E-cadherin MO (*e-cad-MO*) (Babb and Marrs, 2004) induced a strong reduction in cell-cell adhesion properties of isolated DFCs (see Fig. S4 in the supplementary material). Interestingly, we also found that *e-cad-MO* injection leads to defects in DFC compaction very similar to those observed in *pk1a*-MO embryos, and the same effect was observed when *e-cad-MO* was targeted to the DFCs (see Fig.

S5 in the supplementary material). Importantly, E-cad abrogation in the DFCs also induced defects in KV shape (see Fig. S5 in the supplementary material) and heart loop laterality (see Fig. S4 in the supplementary material) that phenocopied Wnt11 and Pk1a loss-of-function, further supporting a key role for cell adhesion properties during KV organogenesis. Previous reports have shown that PCP signalling regulates E-cadherin in different cellular contexts (Classen et al., 2005; Ulrich et al., 2005). In agreement with this, we observed that injection of *e-cad-MO* into the DFCs of *slb* mutant embryos enhanced the defects in KV formation and heart loop laterality (see Figs S4 and S5 in the supplementary material), suggesting that Wnt11- and Pk1a-mediated PCP signalling and cadherin molecules have partially redundant functions during KV organogenesis.

## DISCUSSION

Our analyses indicate that PCP signalling coordinates the genesis of KV organ shape by regulating calcium-dependent cell adhesion properties in progenitor DFCs. This result is consistent with previous findings showing that PCP signalling regulates cadherin dynamics (Classen et al., 2005; Ulrich et al., 2005), adherens junctions (Lindqvist et al., 2010) and intracellular  $\text{Ca}^{2+}$  levels (Veeman et al., 2003) in zebrafish, and a report showing that pharmacological manipulation of intracellular  $\text{Ca}^{2+}$  release

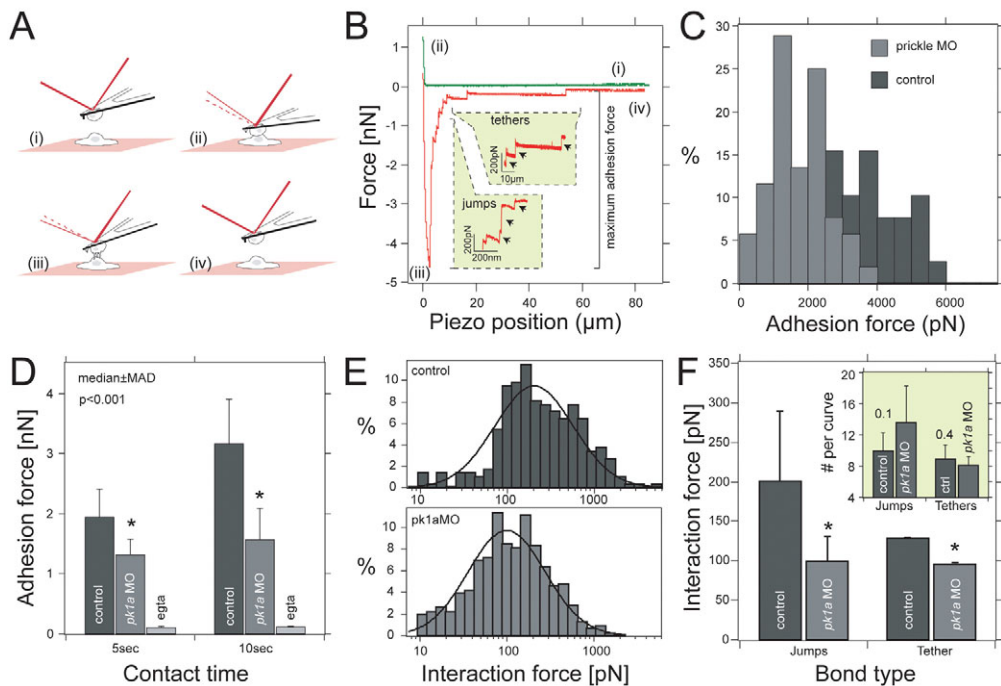


**Fig. 6. *Pk1a* regulates cell adhesion properties between DFCs.** (A) Schematic outline of the single-cell force spectroscopy. Two cells are approached (i) until they come into contact (ii) to establish adhesion (i,ii). After the preset contact time, both cells are withdrawn (iii) until they are completely separate again (iv). (B) Representative force-distance curves taken from control DFCs. Unbinding events are separated into 'jumps' and 'tethers'. Both are shown in separate insets. For data analysis, we quantified maximum adhesion force, jump and tether force. (C) Frequency distribution of adhesion forces recorded from control ( $n \approx 30$  cells; dark grey) and *pk1a*-MO ( $n \approx 35$  cells; light grey) DFCs for 10 seconds contact time. (D) Median  $\pm$  median absolute deviation (m.a.d.) of the maximum adhesion force for control and *pk1a*-MO DFCs in control and calcium suppression conditions (EGTA). \*,  $P < 0.01$ , Mann-Whitney  $U$ -test. (E) Frequency distribution of jumps quantified from force curves taken with control ( $n = 296$  events; top) and *pk1a*-MO ( $n = 469$  events; bottom) cells. Distributions were fitted to Equation 1 (see Materials and methods) to extract the average force step size. (F) Mean force and standard error for jumps and tethers extracted for 10 seconds contact time measured in control and *pk1a*-MO DFCs. \*,  $P < 0.001$ , Mann-Whitney  $U$ -test. Inset shows the average number of jumps and tethers extracted from a log-normal distribution.

induces defects in DFC migration and coalescence (Schneider et al., 2008). Direct measurement of the interaction forces between isolated DFCs revealed a strong reduction in cell-cell adhesion forces after abrogation of *Pk1a* function. Quantification of individual unbinding events in SCFS (jumps or tethers) (Panorchan et al., 2006; Taubenberger et al., 2007; Tulla et al., 2008) also revealed that defective cell-cell adhesion is accompanied by an increased number of jumps and a significant reduction in the average force at which these cytoskeleton-coupled adhesion events break compared with controls. These observations strongly suggest that cooperativity among adhesion molecules is partially lost in PCP-impaired DFCs. Cooperativity of cell adhesion molecules can, in principle, be achieved by their lateral clustering to adhesive plaques (Selhuber-Unkel et al., 2010; Zhang et al., 2009), the diffusion of receptors in the plane of the membrane (Yauch et al., 1997) or the delivery of new adhesion molecules into the zone of contact by exocytosis (Wirtz-Peitz and Zallen, 2009). In support of the latter, PCP signalling has been shown to regulate the dynamics of calcium-dependent cell adhesion molecules through the modulation of GTPases of the Rab family (Classen et al., 2005; Ulrich et al., 2005). Interestingly, our results also showed a reduced tether force in PCP-deficient DFCs. It is known that membrane tension directly influences the extrusion force of tethers from the cell membrane (Hochmuth and Evans, 1982); therefore, reduction in tether forces suggests that membrane tension might be affected in DFCs. As

membrane tension has been proposed to regulate the mobility of membrane proteins and hence their clustering at the plasma membrane (Delanoe-Ayari et al., 2004; Oghalai et al., 2000), it is possible that tension might play a role in the reduced cell-cell adhesion properties of PCP-impaired DFCs. Further analyses will be needed to clarify this possibility.

In zebrafish, PCP-signalling appears to play a fundamental role in both the acquisition of a proper laterality organ shape (this study) and in ciliogenesis (Oishi et al., 2006) (this study). Interestingly, different shapes and geometries of ciliated organs in mammals, amphibians and teleosts are associated with distinct spatial patterns of Nodal flow (Okada et al., 2005; Schweickert et al., 2007). These observations suggest that an effective Nodal flow not only depends on cilia beating (Hirokawa et al., 2006) but also in the acquisition of a defined organ shape. Importantly, our previous analyses showed that KV lumen formation and cilia development are temporally coupled processes (Oteiza et al., 2008). In this study, we have extended these observations to reveal that PCP-mediated cell adhesion regulates the acquisition of organ shape and that this process, in turn, is mechanistically coupled to KV lumen formation and cilia development. From our results, we conclude that PCP-dependent adhesion does not control the initial polarisation and attachment of DFCs to the EVL (Fig. 4B,B'). In addition, PCP signalling does not appear to be required for rosette formation per se (Fig. 4D,D'). Instead, we propose that PCP-dependent adhesion regulates the convergence and organisation of

progenitor cells within the cluster, allowing the gradual translocation of DFCs towards the centre of the rosette and forming lumen. In this context, defective cell adhesion reduces the number and rate at which DFCs become positioned at the lumen side, resulting in a reduced contribution of apical membrane to the forming lumen, which finally results in a decreased KV volume growth (Fig. 5). Intracellular vacuole-like structures that fuse with the apical membrane of lumen-facing DFCs have been implicated in KV lumen formation and expansion (Oteiza et al., 2008) in a way reminiscent of lumen formation in blood vessels (Kamei et al., 2006). Given the reduced number of lumen-facing DFCs, a decreased amount of fused vacuoles might account for the delayed KV lumen growth observed in PCP-defective embryos. In the same context, the diminished number of lumen-forming DFCs appears to account for the decreased cilia number, as these two features are correlated in both control and in PCP-defective embryos (data not shown). Nevertheless, it is still possible that cilia growth is regulated by a different mechanism. A previous report showed that a Dishevelled (Dsh)-mediated PCP signalling pathway regulates cilia development in the KV through cortical actin organisation (Oishi et al., 2006). By contrast, we did not observe significant changes in cortical actin in lumen-facing DFCs of *pk1a-MO* embryos (see Fig. S1 in the supplementary material), suggesting that Wnt11- and Pk1a-mediated PCP signalling might regulate cilia formation in the KV by a Dsh-independent mechanism. More recently, it has been proposed that a Vangl2-dependent PCP pathway regulates cilia polarisation in the KV (Borovina et al., 2010) and, in addition, *Vangl2* mutant embryos show increased KV lumen size compared with controls (Borovina et al., 2010). As Prickle and Vangl2 have been shown to interact both biochemically and genetically (Jenny et al., 2003), these results suggest that a correct balance between components of the PCP pathway might play a key role in the regulation of KV morphogenesis and cilia formation. Whether PCP-signalling controls lumen formation and ciliogenesis directly, or whether it does it indirectly through the regulation of cell adhesion properties, remains to be tested.

This study provides a clear example of how cell adhesion-mediated processes in progenitor cells coordinate vertebrate organogenesis. How other mechanical features of DFCs participate in KV formation is still unknown. Interestingly, DFC migration and rosette formation seem to depend on their attachment to the EVL (Oteiza et al., 2008) (P.O., E.P. and M.L.C., unpublished). Hence, it is tempting to speculate that mechanical forces exerted by the pulling of the outer epithelium play a role during KV morphogenesis. Further genetic and biophysical studies will be needed to test this hypothesis and describe the network of mechanical forces acting during KV organ morphogenesis.

#### Acknowledgements

We are grateful to P. Tomancak for generous manpower support, to J. Peychl for microscopy advice, to E. Lehmann, J. Hückmann, A. Chamorro and L. Cifuentes for fish care and to Y. Arboleda, S. Schneider, R. Pérez and A. Catenaccio for technical help. This work was supported by grants from Mecesup (UCH0306) and DAAD to P.O.; DFG, MPG and the EU to C.-P.H.; and CONICYT (PBCT ACT47), MIDEPLAN (ICM P07-048-F), the Howard Hughes Medical Institute (INTNL55005940) and the EU (FP6-NEST-PATH EDCBNL) to M.L.C.

#### Competing interests statement

The authors declare no competing financial interests.

#### Supplementary material

Supplementary material for this article is available at <http://dev.biologists.org/lookup/suppl/doi:10.1242/dev.049981/-DC1>

#### References

- Amack, J. D. and Yost, H. J.** (2004). The T box transcription factor no tail in ciliated cells controls zebrafish left-right asymmetry. *Curr. Biol.* **14**, 685-690.
- Amack, J. D., Wang, X. and Yost, H. J.** (2007). Two T-box genes play independent and cooperative roles to regulate morphogenesis of ciliated Kupffer's vesicle in zebrafish. *Dev. Biol.* **310**, 196-210.
- Babb, S. G. and Marrs, J. A.** (2004). E-cadherin regulates cell movements and tissue formation in early zebrafish embryos. *Dev. Dyn.* **230**, 263-277.
- Barth, K. A. and Wilson, S. W.** (1995). Expression of zebrafish nk2.2 is influenced by sonic hedgehog/vertebrate hedgehog-1 and demarcates a zone of neuronal differentiation in the embryonic forebrain. *Development* **121**, 1755-1768.
- Blum, M., Andre, P., Muders, K., Schweickert, A., Fischer, A., Bitzer, E., Bogusch, S., Beyer, T., van Straaten, H. W. and Viebahn, C.** (2007). Ciliation and gene expression distinguish between node and posterior notochord in the mammalian embryo. *Differentiation* **75**, 133-146.
- Borovina, A., Superina, S., Voskas, D. and Ciruna, B.** (2010). Vangl2 directs the posterior tilting and asymmetric localization of motile primary cilia. *Nat. Cell Biol.* **4**, 407-412.
- Brown, N. A. and Wolpert, L.** (1990). The development of handedness in left/right asymmetry. *Development* **109**, 1-9.
- Bryant, D. M. and Mostov, K. E.** (2008). From cells to organs: building polarized tissue. *Nat. Rev. Mol. Cell Biol.* **9**, 887-901.
- Carreira-Barbosa, F., Concha, M. L., Takeuchi, M., Ueno, N., Wilson, S. W. and Tada, M.** (2003). Prickle 1 regulates cell movements during gastrulation and neuronal migration in zebrafish. *Development* **130**, 4037-4046.
- Classen, A. K., Anderson, K. I., Marois, E. and Eaton, S.** (2005). Hexagonal packing of *Drosophila* wing epithelial cells by the planar cell polarity pathway. *Dev. Cell* **9**, 805-817.
- Cooper, M. S., Szeto, D. P., Sommers-Herivel, G., Topczewski, J., Solnica-Krezel, L., Kang, H. C., Johnson, I. and Kimelman, D.** (2005). Visualizing morphogenesis in transgenic zebrafish embryos using BODIPY TR methyl ester dye as a vital counterstain for GFP. *Dev. Dyn.* **232**, 359-368.
- D'Amico, L. A. and Cooper, M. S.** (1997). Spatially distinct domains of cell behavior in the zebrafish organizer region. *Biochem. Cell Biol.* **75**, 563-577.
- Delanoe-Ayari, H., Al Kurdi, R., Vallade, M., Gulino-Debrac, D. and Riveline, D.** (2004). Membrane and acto-myosin tension promote clustering of adhesion proteins. *Proc. Natl. Acad. Sci. USA* **101**, 2229-2234.
- Echeverri, K. and Oates, A. C.** (2007). Coordination of symmetric cyclic gene expression during somitogenesis by Suppressor of Hairless involves regulation of retinoic acid catabolism. *Dev. Biol.* **301**, 388-403.
- Essner, J. J., Amack, J. D., Nyholm, M. K., Harris, E. B. and Yost, H. J.** (2005). Kupffer's vesicle is a ciliated organ of asymmetry in the zebrafish embryo that initiates left-right development of the brain, heart and gut. *Development* **132**, 1247-1260.
- Evans, E.** (2001). Probing the relation between force-lifetime and chemistry in single molecular bonds. *Annu. Rev. Biophys. Biomol. Struct.* **30**, 105-128.
- Evans, E., Heinrich, V., Leung, A. and Kinoshita, K.** (2005). Nano- to microscale dynamics of P-selectin detachment from leukocyte interfaces. I. Membrane separation from the cytoskeleton. *Biophys. J.* **88**, 2288-2298.
- Halbleib, J. M. and Nelson, W. J.** (2006). Cadherins in development: cell adhesion, sorting, and tissue morphogenesis. *Genes Dev.* **20**, 3199-3214.
- Hamada, H., Meno, C., Watanabe, D. and Saijoh, Y.** (2002). Establishment of vertebrate left-right asymmetry. *Nat. Rev. Genet.* **3**, 103-113.
- Hammerschmidt, M., Pelegri, F., Mullins, M. C., Kane, D. A., Brand, M., van Eeden, F. J., Furutani-Seiki, M., Granato, M., Haffter, P., Heisenberg, C. P. et al.** (1996). Mutations affecting morphogenesis during gastrulation and tail formation in the zebrafish, *Danio rerio*. *Development* **123**, 143-151.
- Heisenberg, C. P., Brand, M., Jiang, Y. J., Warga, R. M., Beuchle, D., van Eeden, F. J., Furutani-Seiki, M., Granato, M., Haffter, P., Hammerschmidt, M. et al.** (1996). Genes involved in forebrain development in the zebrafish, *Danio rerio*. *Development* **123**, 191-203.
- Heisenberg, C. P., Tada, M., Rauch, G. J., Saude, L., Concha, M. L., Geisler, R., Stemple, D. L., Smith, J. C. and Wilson, S. W.** (2000). Silberblick/Wnt11 mediates convergent extension movements during zebrafish gastrulation. *Nature* **405**, 76-81.
- Hirokawa, N., Tanaka, Y., Okada, Y. and Takeda, S.** (2006). Nodal flow and the generation of left-right asymmetry. *Cell* **125**, 33-45.
- Hochmuth, R. M. and Evans, E. A.** (1982). Extensional flow of erythrocyte membrane from cell body to elastic tether. I. Analysis. *Biophys. J.* **39**, 71-81.
- Jenny, A., Darken, R. S., Wilson, P. A. and Mlodzik, M.** (2003). Prickle and Strabismus form a functional complex to generate a correct axis during planar cell polarity signaling. *EMBO J.* **22**, 4409-4420.
- Kamei, M., Saunders, W. B., Bayless, K. J., Dye, L., Davis, G. E. and Weinstein, B. M.** (2006). Endothelial tubes assemble from intracellular vacuoles in vivo. *Nature* **442**, 453-456.
- Kane, D. A., McFarland, K. N. and Warga, R. M.** (2005). Mutations in half baked/E-cadherin block cell behaviors that are necessary for teleost epiboly. *Development* **132**, 1105-1116.

- Kilian, B., Mansukoski, H., Barbosa, F. C., Ulrich, F., Tada, M. and Heisenberg, C. P.** (2003). The role of Ppt/Wnt5 in regulating cell shape and movement during zebrafish gastrulation. *Mech. Dev.* **120**, 467-476.
- Kimmel, C. B., Ballard, W. W., Kimmel, S. R., Ullmann, B. and Schilling, T. F.** (1995). Stages of embryonic development of the zebrafish. *Dev. Dyn.* **203**, 253-310.
- Koppen, M., Fernandez, B. G., Carvalho, L., Jacinto, A. and Heisenberg, C. P.** (2006). Coordinated cell-shape changes control epithelial movement in zebrafish and *Drosophila*. *Development* **133**, 2671-2681.
- Kramer-Zucker, A. G., Olale, F., Haycraft, C. J., Yoder, B. K., Schier, A. F. and Drummond, I. A.** (2005). Cilia-driven fluid flow in the zebrafish pronephros, brain and Kupffer's vesicle is required for normal organogenesis. *Development* **132**, 1907-1921.
- Krieg, M., Arboleda-Estudillo, Y., Puech, P. H., Kafer, J., Graner, F., Muller, D. J. and Heisenberg, C. P.** (2008). Tensile forces govern germ-layer organization in zebrafish. *Nat. Cell Biol.* **10**, 429-436.
- Lindqvist, M., Horn, Z., Bryja, V., Schulte, G., Papachristou, P., Ajima, R., Dyberg, C., Arenas, E., Yamaguchi, T. P., Lagercrantz, H. et al.** (2010). Vang-like protein 2 and Rac1 interact to regulate adherens junctions. *J. Cell Sci.* **123**, 472-483.
- Long, S., Ahmad, N. and Rebagliati, M.** (2003). The zebrafish nodal-related gene southpaw is required for visceral and diencephalic left-right asymmetry. *Development* **130**, 2303-2316.
- Muller, D. J., Helenius, J., Alsteens, D. and Dufrene, Y. F.** (2009). Force probing surfaces of living cells to molecular resolution. *Nat. Chem. Biol.* **5**, 383-390.
- Nonaka, S., Tanaka, Y., Okada, Y., Takeda, S., Harada, A., Kanai, Y., Kido, M. and Hirokawa, N.** (1998). Randomization of left-right asymmetry due to loss of nodal cilia generating leftward flow of extraembryonic fluid in mice lacking KIF3B motor protein. *Cell* **95**, 829-837.
- Nonaka, S., Shiratori, H., Saijoh, Y. and Hamada, H.** (2002). Determination of left-right patterning of the mouse embryo by artificial nodal flow. *Nature* **418**, 96-99.
- Oghalai, J. S., Zhao, H. B., Kutz, J. W. and Brownell, W. E.** (2000). Voltage- and tension-dependent lipid mobility in the outer hair cell plasma membrane. *Science* **287**, 658-661.
- Oishi, I., Kawakami, Y., Raya, A., Callol-Massot, C. and Izpisua Belmonte, J. C.** (2006). Regulation of primary cilia formation and left-right patterning in zebrafish by a noncanonical Wnt signaling mediator, duboraya. *Nat. Genet.* **38**, 1316-1322.
- Okada, Y., Takeda, S., Tanaka, Y., Belmonte, J. C. and Hirokawa, N.** (2005). Mechanism of nodal flow: a conserved symmetry breaking event in left-right axis determination. *Cell* **121**, 633-644.
- Oteiza, P., Koppen, M., Concha, M. L. and Heisenberg, C. P.** (2008). Origin and shaping of the laterality organ in zebrafish. *Development* **135**, 2807-2813.
- Panorchan, P., Thompson, M. S., Davis, K. J., Tseng, Y., Konstantopoulos, K. and Wirtz, D.** (2006). Single-molecule analysis of cadherin-mediated cell-cell adhesion. *J. Cell Sci.* **119**, 66-74.
- Puech, P. H., Poole, K., Knebel, D. and Muller, D. J.** (2006). A new technical approach to quantify cell-cell adhesion forces by AFM. *Ultramicroscopy* **106**, 637-644.
- Sakaguchi, T., Kikuchi, Y., Kuroiwa, A., Takeda, H. and Stainier, D. Y.** (2006). The yolk syncytial layer regulates myocardial migration by influencing extracellular matrix assembly in zebrafish. *Development* **133**, 4063-4072.
- Schneider, I., Houston, D. W., Rebagliati, M. R. and Slusarski, D. C.** (2008). Calcium fluxes in dorsal forerunner cells antagonize  $\beta$ -catenin and alter left-right patterning. *Development* **135**, 75-84.
- Schweickert, A., Weber, T., Beyer, T., Vick, P., Bogusch, S., Feistel, K. and Blum, M.** (2007). Cilia-driven leftward flow determines laterality in *Xenopus*. *Curr. Biol.* **17**, 60-66.
- Seifert, J. R. and Mlodzik, M.** (2007). Frizzled/PCP signalling: a conserved mechanism regulating cell polarity and directed motility. *Nat. Rev. Genet.* **8**, 126-138.
- Selhuber-Unkel, C., Erdmann, T., Lopez-Garcia, M., Kessler, H., Schwarz, U. S. and Spatz, J. P.** (2010). Cell adhesion strength is controlled by intermolecular spacing of adhesion receptors. *Biophys. J.* **98**, 543-551.
- Sheetz, M. P.** (2001). Cell control by membrane-cytoskeleton adhesion. *Nat. Rev. Mol. Cell Biol.* **2**, 392-396.
- Solnica-Krezel, L.** (2006). Gastrulation in zebrafish – all just about adhesion? *Curr. Opin. Genet. Dev.* **16**, 433-441.
- Sun, M., Northup, N., Marga, F., Huber, T., Byfield, F. J., Levitan, I. and Forgacs, G.** (2007). The effect of cellular cholesterol on membrane-cytoskeleton adhesion. *J. Cell Sci.* **120**, 2223-2231.
- Taubenberger, A., Cisneros, D. A., Friedrichs, J., Puech, P. H., Muller, D. J. and Franz, C. M.** (2007). Revealing early steps of alpha2beta1 integrin-mediated adhesion to collagen type I by using single-cell force spectroscopy. *Mol. Biol. Cell* **18**, 1634-1644.
- Tulla, M., Helenius, J., Jokinen, J., Taubenberger, A., Muller, D. J. and Heino, J.** (2008). TPA primes alpha2beta1 integrins for cell adhesion. *FEBS Lett.* **582**, 3520-3524.
- Ulrich, F., Krieg, M., Schotz, E. M., Link, V., Castanon, I., Schnabel, V., Taubenberger, A., Mueller, D., Puech, P. H. and Heisenberg, C. P.** (2005). Wnt11 functions in gastrulation by controlling cell cohesion through Rab5c and E-cadherin. *Dev. Cell* **9**, 555-564.
- Veeman, M. T., Slusarski, D. C., Kaykas, A., Louie, S. H. and Moon, R. T.** (2003). Zebrafish prickle, a modulator of noncanonical Wnt/Fz signaling, regulates gastrulation movements. *Curr. Biol.* **13**, 680-685.
- Wang, Y. and Nathans, J.** (2007). Tissue/planar cell polarity in vertebrates: new insights and new questions. *Development* **134**, 647-658.
- Wirtz-Peitz, F. and Zallen, J. A.** (2009). Junctional trafficking and epithelial morphogenesis. *Curr. Opin. Genet. Dev.* **19**, 350-356.
- Wolpert, L.** (2002). *Principles of Development*. Oxford: Oxford University Press.
- Yauch, R. L., Felsenfeld, D. P., Kraeft, S. K., Chen, L. B., Sheetz, M. P. and Hemler, M. E.** (1997). Mutational evidence for control of cell adhesion through integrin diffusion/clustering, independent of ligand binding. *J. Exp. Med.* **186**, 1347-1355.
- Zallen, J. A.** (2007). Planar polarity and tissue morphogenesis. *Cell* **129**, 1051-1063.
- Zhang, Y., Sivasankar, S., Nelson, W. J. and Chu, S.** (2009). Resolving cadherin interactions and binding cooperativity at the single-molecule level. *Proc. Natl. Acad. Sci. USA* **106**, 109-114.